Circular photonic crystal fiber supporting 118 orbital angular momentum modes transmission

Haihao Fu,[a] Chao Liu,[a,*] Chunjie Hu,[b] Lei Zhou,[c] Ying Shi,[d] Jingwei Lv,[a] Lin Yang,[a] and Paul K. Chu[e]

[a]Northeast Petroleum University, Daqing, China
[b]The Fourth Affiliated Hospital of Harbin Medical University, Department of Gynaecology and Obstetrics, Harbin, China
[c]The Second Affiliated Hospital of Harbin Medical University, Department of Orthopedics, Harbin, China
[d]Northeast Petroleum University, Institute of Unconventional Oil & Gas, Daqing, China
[e]City University of Hong Kong, Department of Physics, Department of Materials Science and Engineering, and Department of Biomedical Engineering, Kowloon, China

Abstract. Circular photonic crystal fiber consisting of doped amethyst and big and small round air holes is designed to support transmission of 118 orbital angular momentum (OAM) modes in the range of 1.2 to 1.65 μm. Numerical analysis by the finite element method (FEM) reveals that the effective index difference of all the modes are larger than 1×10^{-4}, which can propagate OAM modes stably. The nonlinear coefficient is 0.583 $W^{-1}\,km^{-1}$ at 1.55 μm, which is very low and helps to reduce mode coupling. In addition, the confinement loss of the eigenmode is between 10^{-12} and 10^{-8} dB/m. The dispersion is very flat for the low-order mode $HE_{1,1}$, for which the dispersion variation is just 1.459 ps/(km nm). This fiber has great potential in stable and large-capacity mode propagation in optical communication. © *2021 Society of Photo-Optical Instrumentation Engineers (SPIE)* [DOI: 10.1117/1.OE.60.7.076102]

Keywords: orbital angular momentum; photonic crystal fiber; optical communication; nonlinear coefficient.

Paper 20210318 received Mar. 23, 2021; accepted for publication Jun. 22, 2021; published online Jul. 7, 2021.

1 Introduction

Space division multiplexing is a communication technique that combines a series of optical signals of different wavelengths, transmits them along a single optical fiber, and separates them at the receiving end. It is widely used in large-capacity communication and can overcome the capacity limitation plaguing present optical communication systems.[1] To improve optical fiber communication, transmission of as many modes as possible is the goal and has become a hot research topic. In this respect, orbital angular momentum (OAM) mode multiplexing in optical fibers can increase the communication capacity.[2] However, the OAM beam cannot propagate stably in traditional optical fibers, on account of the degeneracy of the constituents for the OAM. Therefore, it is important to design a special optical fiber structure that can support large-capacity OAM propagation. Owing to the helical wavefront phase form of $e^{\pm il\theta}$, where l is topological charge number and θ is azimuth, OAM consists of infinite orthogonal modes when l is substituted with any integer. OAM is a new dimension of optical fiber communication. The OAM modes propagated in photonic crystal fiber (PCF) can be defined as the superposition of odd and even modes of vector modes with of the same order. $OAM^{\pm}_{\pm l,m}$ is composed of HE^{even}_{l+1} and HE^{odd}_{l+1}, or EH^{even}_{l-1} and EH^{odd}_{l-1}. HE^{even} or EH^{even} is the even HE and EH modes, and HE^{odd} or EH^{odd} is the odd mode of HE and EH modes, respectively. The principle of composition is expressed in the following two formulas:[3]

*Address all correspondence to Chao Liu, msm-liu@126.com

0091-3286/2021/$28.00 © 2021 SPIE

$$\mathrm{OAM}^{\pm}_{\pm l,m} = \mathrm{HE}^{\mathrm{even}}_{l+1,m} \pm i\mathrm{HE}^{\mathrm{odd}}_{l+1,m} \quad \text{and} \quad \mathrm{OAM}^{\mp}_{\pm l,m} = \mathrm{EH}^{\mathrm{even}}_{l-1,m} \pm i\mathrm{EH}^{\mathrm{odd}}_{l-1,m}, \tag{1}$$

where l is an integer termed the topological charge number and m is the radial order which is usually substituted as $m = 1$ to simplify reuse and demultiplexing of the OAM mode. The sign in the superscript "$\pm$" denotes the right or left circular polarization and that of $\pm l$ denotes the right or left wave front rotation direction. The OAM modes not only have the same and reverse polarization but rotation direction when $l \geq 2$ is the result of four independent information states.[4] Therefore, each $\mathrm{OAM}^{\pm}_{\pm l,m}$ ($l \geq 2$) mode group contains four OAM states, meaning that a topological charge number can represent four OAM modes. However, when $l = 1$, it can only be used as two information states because the $\mathrm{OAM}_{\pm 1,1}$ has identical circular polarization and rotation direction.

The PCF has advantages such as the large mode area, low loss, low nonlinearity, and so on, and can be adopted to transmit OAM modes. However, the OAM beam cannot propagate stably until the effective index difference is greater than 10^{-4}.[5] Recently, different kinds of fibers with the ring-core structure which can support OAM transmission have been proposed. Yue et al.[6] reported an annular PCF based on As_2S_3 in 2012 and a high effective index difference was observed. Unfortunately, this fiber only supported two modes. Li et al.[7] presented a kagome PCF that supported three OAM modes and Nandam and Shin described an PCF which could transmit 14 OAM modes.[8] In 2016, Zhang designed a circular PCF that supported transmission of 26 OAM modes and the chromatic dispersion for the OAM modes was within 39 $\mathrm{ps}/(\mathrm{nm\,km})$ over a bandwidth of 750 nm.[9] Wang et al. designed an PCF with mixed air holes which could propagate 34 OAM modes[10] and another PCF was reported to transmit 58 OAM modes.[11] Recently, an PCF consisting of doped amethyst ($n = 1.55$) was proposed by Zhang et al.[12] to transmit 110 OAM modes. This PCF design appears to have the largest number of transmission modes and to increase the number of OAM modes, efforts have been devoted to reduce mode coupling in the PCF.

Herein, we present a new circular PCF structure consisting of doped amethyst and mixed big and small round air holes for transmission of 118 OAM modes in the range between 1.2 and 1.65 μm. The effective index difference of the fiber is larger than 10^{-4}. This structure has not only a large mode field area (184.88 $\mu\mathrm{m}^2$) and low nonlinear coefficient (0.583 $\mathrm{W}^{-1}\,\mathrm{km}^{-1}$), but also confinement losses between 10^{-12} and 10^{-8} dB/m.

2 PCF Design and Numerical Simulation

To achieve large-capacity mode transmission in optical fiber communication, the new PCF is shown in Fig. 1. The structure with doped amethyst ($n = 1.55$) is quite different from existing optical fibers. Amethyst doping in the purple area not only improves the effective refractive index difference between adjacent modes, but also greatly increases the number of OAM modes

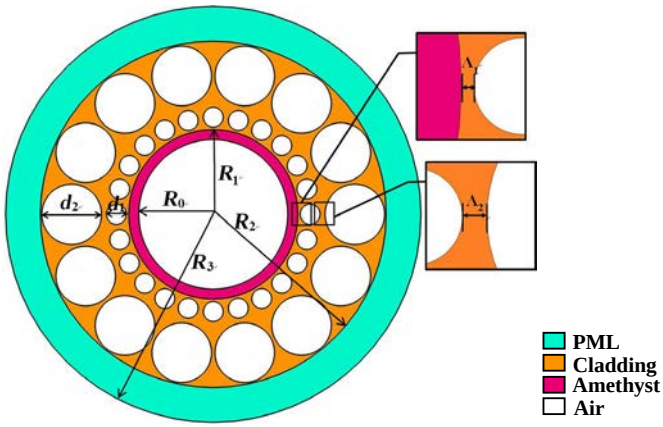

Fig. 1 Cross-section of the annular index profile structure in the photonic crystal fiber.

that can be propagated stably. The orange area is the silica cladding of the fiber and the core of the fiber is a big hole filled with air. There are two layers of circular air holes in the cladding. The reason for the two layers of air holes is that they can prevent the higher-order modes from leaking to the cladding. The blue region is the perfectly matched layer (PML) constituting the boundary conditions. In addition, the optical fiber can be prepared by sol-gel method.[13] The specific manufacturing process is as follows:[14] under the action of catalyst, the material is hydrolyzed and condensed to form sol, and then the gel is obtained after aging. The SiO_2 powder can be formed by gel heat treatment and be made into fiber preform, which is eventually pulled into fiber by melt quenching. This method can remarkably reduce the manufacturing difficulty, and it can freely adjust the size, shape, and spacing of the air holes, thus it is suitable for the proposed structure of PCF in this work. In addition, after the formation of SiO_2 powder, the melting point of amethyst is higher than that of SiO_2, leading to that it can be directly doped. Consequently, the possibility of doping amethyst by means of this technology is desired.

The refractive index of the background materials and PML depends on the Sellmeier equation [15] as Eq. (2):

$$n^2(\lambda) = 1 + \frac{A_1\lambda^2}{\lambda^2 - B_1} + \frac{A_2\lambda^2}{\lambda^2 - B_2} + \frac{A_3\lambda^2}{\lambda^2 - B_3}, \tag{2}$$

where $A_1 = 0.6961663$, $A_2 = 0.4079426$, $A_3 = 0.897479$, $B_1 = 0.0684043$, $B_2 = 0.1162414$, and $B_3 = 9.896161$. The limitation ability of the circular area to OAM modes is advanced with increasing radius of the ring transmission area R_1 and the number of OAM modes increases rapidly. Additionally, the effective index difference increases and the confinement loss decreases when the ratio of the diameters (d_1/d_2) of the inner and outer circular air holes is reduced. COMSOL is used in the simulation for the range of $10\ \mu\text{m} < R_0$, $R_1 < 18\ \mu\text{m}$, $0\ \mu\text{m} < d_1 < 5\ \mu\text{m}$, and $10\ \mu\text{m} < d_2 < 15\ \mu\text{m}$. During the simulation calculation, the number of OAM modes increases with increasing R_0, and the number of OAM modes reaches the maximum for $R_0 = 15\ \mu\text{m}$. The thickness of the annular region is determined by $R_1 - R_0$. The larger the R_1 is, the thicker the annular region is and the smaller the dispersion is. However, when R_1 is larger than $17\ \mu\text{m}$, the number of OAM modes begins to decrease, and the effective index difference is the largest for $d_1 = 4\ \mu\text{m}$ and $d_2 = 12\ \mu\text{m}$. In addition, the confinement loss of the PCF can be minimized for $\Lambda_1 = 0.5\ \mu\text{m}$ and $\Lambda_2 = 1\ \mu\text{m}$. PML determined by R_2 and R_3 is set as boundary condition and has no effect on the proposed PCF. Consequently, we set $R_0 = 15\ \mu\text{m}$, $R_1 = 17\ \mu\text{m}$, $R_2 = 34.8\ \mu\text{m}$, $R_3 = 41.8\ \mu\text{m}$, $d_1 = 4\ \mu\text{m}$, and $d_2 = 12\ \mu\text{m}$. The distance between the doped layer and first layer of the air holes is $\Lambda_1 = 0.5\ \mu\text{m}$ and the gap between the two layers of circular air holes is $\Lambda_2 = 1\ \mu\text{m}$. As in an annular ring fiber, the OAM modes are transmitted in the ring area between the central air hole and cladding air hole arrays.

3 Results and Discussion

3.1 *Transmitted Modes*

According to theory, the OAM modes are composed of HE and EH modes. HE and EH modes will appear when COMSOL is used in the simulation. According to the relationship between the refractive index of the medium and the transmission speed of the light wave, the refractive index of the HE modes are greater than that of the EH modes at the same wavelength and the order of OAM. The topological charge of the HE module can reach 31 and that of EH is up to 29 in an advanced structure. Consequently, the fiber described here can propagate $29 \times 4 + 2 = 118$ OAM modes from 1.2 to 1.65 μm according to Eq. (1).

Figures 2(a)–2(f) and 2(g)–2(l) describe the optical field distributions in z direction of the partial HE and EH modes, respectively. Owing to the powerful ability to limit lower order modes, almost all of the energy is concentrated in the annular region. The red and blue regions represent the magnitude of the mode field strength, and the number of pairs in the red blue region corresponds to the order of the pattern. The HE modes are distributed at the outer boundary of the annular region, which is closer to the cladding. EH modes are located in the inner boundary, which is closer to the core. It not only distinguishes the HE modes from the EH modes, but

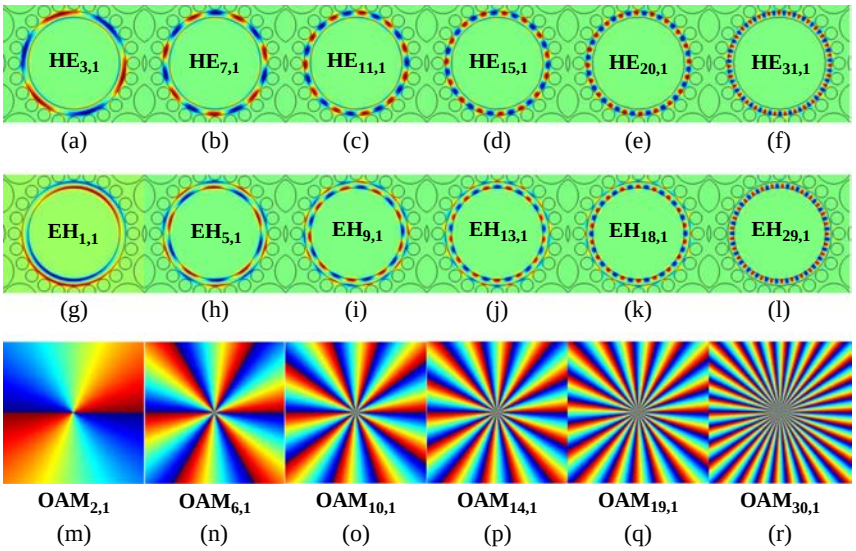

Fig. 2 (a) – (i) Optical field distributions of the partial HE and EH modes; (m) – (r) Phase diagrams of a part of the displayed HE and EH modes.

indicates that the EH modes will be more stable when the fiber is affected by the external environment. In addition, it is seen from the light field distribution that each mode exists light field leakage. Based on the inferior confinement ability to higher order modes, the higher-order modes are easier to leak into the cladding than the lower order modes, thus a certain degree of ring edge serration appears. Figures 2(m) – 2(r) show the phase diagram of the displayed HE and EH modes using MATLAB. Although the phase distribution changes with the topological charge, the phase structure is always helical. The beam rotates around the optical axis once. The phase changes to 4π when the topological charge number is 2 and the phase changes to 24π when the topological charge number is 12. Hence, it can be inferred that when the topological charge number is n, the beam rotates around the optical axis once and the phase changes to $2n\pi$. In addition, the phase distribution of the OAM mode changes $\pi/2$ azimuthally and therefore, we can demultiplex these modes with conjugating phase modes.

32 *Effective Refractive Index*

Whether OAM modes can propagate stably in the fiber depends on the effective refractive index between the HE and EH modes and the OAM of the same order should be larger than 1×10^{-4}. An effective index difference $<1 \times 10^{-4}$ may lead to crosstalk and coupling of different modes forming scalar LP modes.

Figure 3 shows the effective refractive indexes of all the eigenmodes as a function of wavelength from 1.20 to 1.65 μm for this PCF. The mode field energy that is mainly concentrated in the ring region in the annular index profile structure expands gradually to the cladding with increasing wavelength, leading to the effective refractive index reduction. The reason why the effective refractive index of the low-order modes is lower than that of high-order modes is that higher-order modes can leak more easily into the cladding.

The larger the wavelength is, the faster the refractive index decreases, thus the greater the separation of eigenmodes $HE_{l+1,1}$ and $EH_{l-1,1}$, the greater the refractive index difference. Figure 4 shows the relationship between the effective index difference and wavelength. It is seen that the effective refractive index difference is proportional to the wavelength. The OAM mode which has the smallest refractive index difference (1.9×10^{-4}) is $OAM_{30,1}$ at 1.2 μm. Therefore, mode coupling is very small and all the modes can be transmitted stably in the range of 1.2 to 1.65 μm. The refractive index of amethyst is different from that of silica and so the effective index difference can be improved by doping. The largest $OAM_{2,1}$ at 1.65 μm is 3.75×10^{-3} which is much bigger than 1.85×10^{-3} in Ref. 16 and 1.56×10^{-3} in Ref. 17.

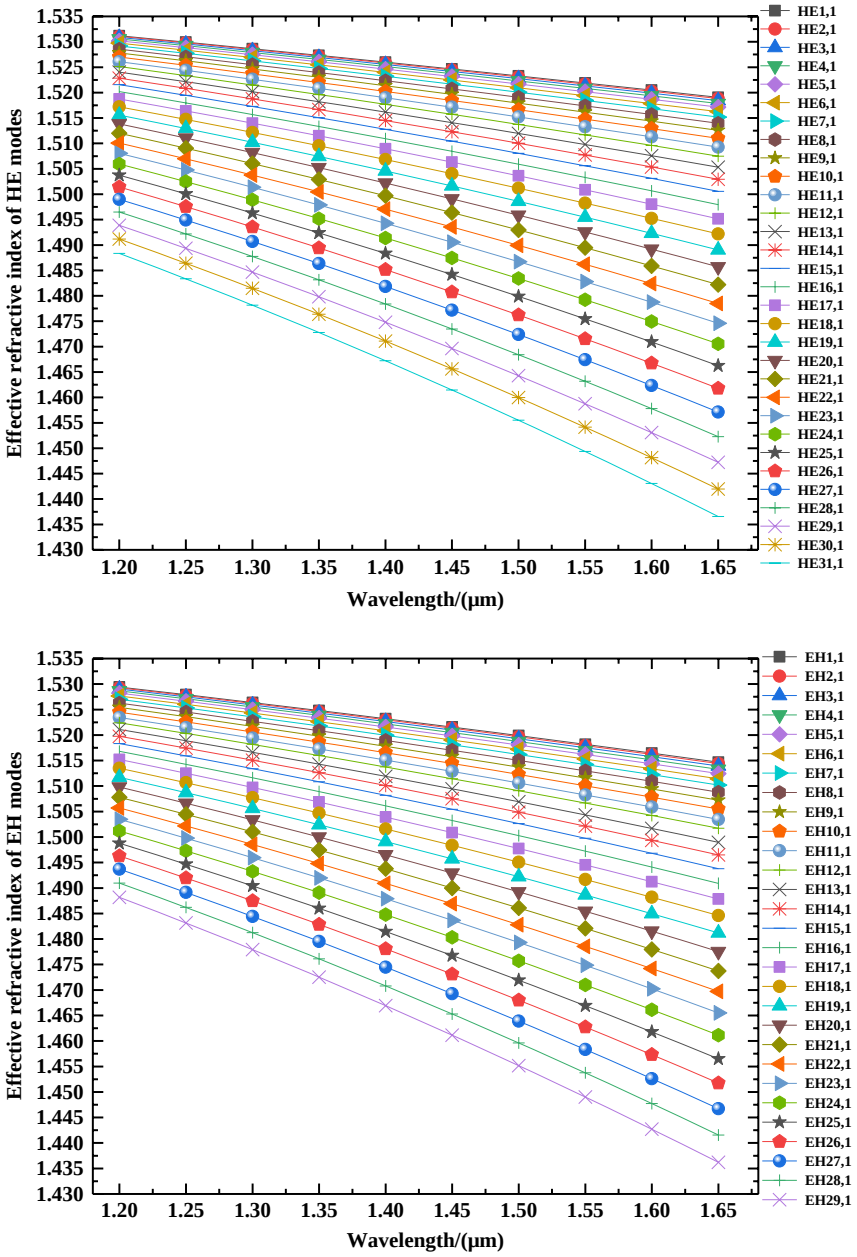

Fig. 3 Effective refractive indexes of the HE modes and EH modes.

3.3 *Chromatic Dispersion*

The phenomenon of different wave speeds caused by different frequencies of light with different wavelengths is called chromatic dispersion which consists of waveguide and materials dispersion. Material dispersion depends on the material itself, and the material dispersion of doping amethyst can be calculated by the single-term Sellmeier equation:[18]

$$\frac{1}{n^2-1} = -\frac{A}{\lambda^2} + B, \tag{3}$$

where $A = 0.0065$ and $B = 0.7359$. The material dispersion of amethyst can be obtained from the second derivative of refractive index with respect to wavelength.

The total dispersion can be obtained by the relationship between the wavelength and effective refractive index[19] shown in Eq. (4):

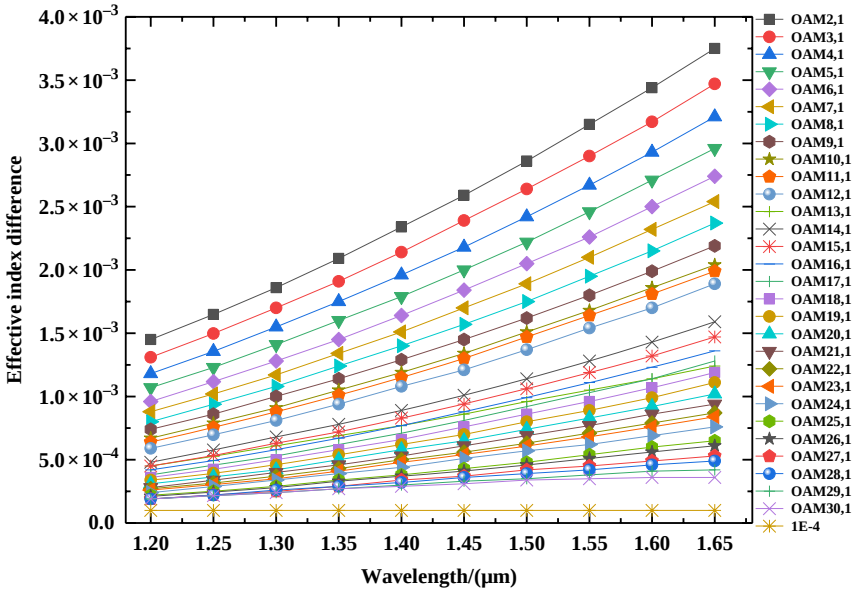

Fig. 4 Effective index difference of the OAM modes.

$$D = -\frac{\lambda}{c}\frac{d^2\mathrm{Re}(n_{\mathrm{eff}})}{d\lambda^2}, \tag{4}$$

where $c = 3 \times 10^8$ m/s is the speed of light and $\mathrm{Re}(n_{\mathrm{eff}})$ is the real part of the effective refractive index. Figure 5 shows the chromatic dispersion variations of the HE modes and EH modes from 1.2 to 1.65 μm. The dispersion of the low-order modes is smaller than that of the high-order modes because the change of effective refractive index of the low-order modes is smaller than that of the higher-order mode as the wavelength increases. It is very flat for the low-order HE modes and EH modes in the figure, particularly $\mathrm{HE}_{1,1}$ which dispersion variation is just 1.459 ps/(km nm) and better than those reported in Refs. 8 and 20 of >15 ps/(km nm). The dispersion of the higher-order modes increases greatly with increasing wavelength, which is not conducive to long-distance transmission of the OAM modes.

3.4 *Effective Mode Area and Nonlinear Coefficients*

The effective mode area refers to the cross-sectional area of the energy concentration region in the optical fiber structure. The effective mode area not only enlarges with increasing wavelength, but also gets bigger when the number of modes is altered. The reason is that the longer the wavelength, the weaker the limitation of the annular region is on the mode field intensity and the beam can leak more easily into the cladding. The formula for the effective mode field area[21] is shown in Eq. (5) and the effective mode areas of the HE and EH modes are shown in Fig. 6:

$$A_{\mathrm{eff}} = \frac{\left(\iint |E(x,y)|^2 \mathrm{d}x\,\mathrm{d}y\right)^2}{\iint |E(x,y)|^4 \mathrm{d}x\,\mathrm{d}y}. \tag{5}$$

Figure 6 shows that the maximum area is 184.88 μm^2 for $\mathrm{HE}_{31,1}$ between 1.2 and 1.65 μm. The remarkably large effective mode area is the biggest advantage of this structure as it is much better than 68.51 μm^2 in Ref. 19 and 35.58 μm^2 in Ref. 17. The nonlinear coefficient, another significant physical parameter reflecting the performance of PCF, is inversely proportional to the effective mode field area. The nonlinear refractive indexes of cladding and annular region are different due to their different materials. Therefore, it is necessary to calculate the nonlinear coefficients respectively. The nonlinear coefficient is determined by Eq. (6)[22] and Eq. (7):[23]

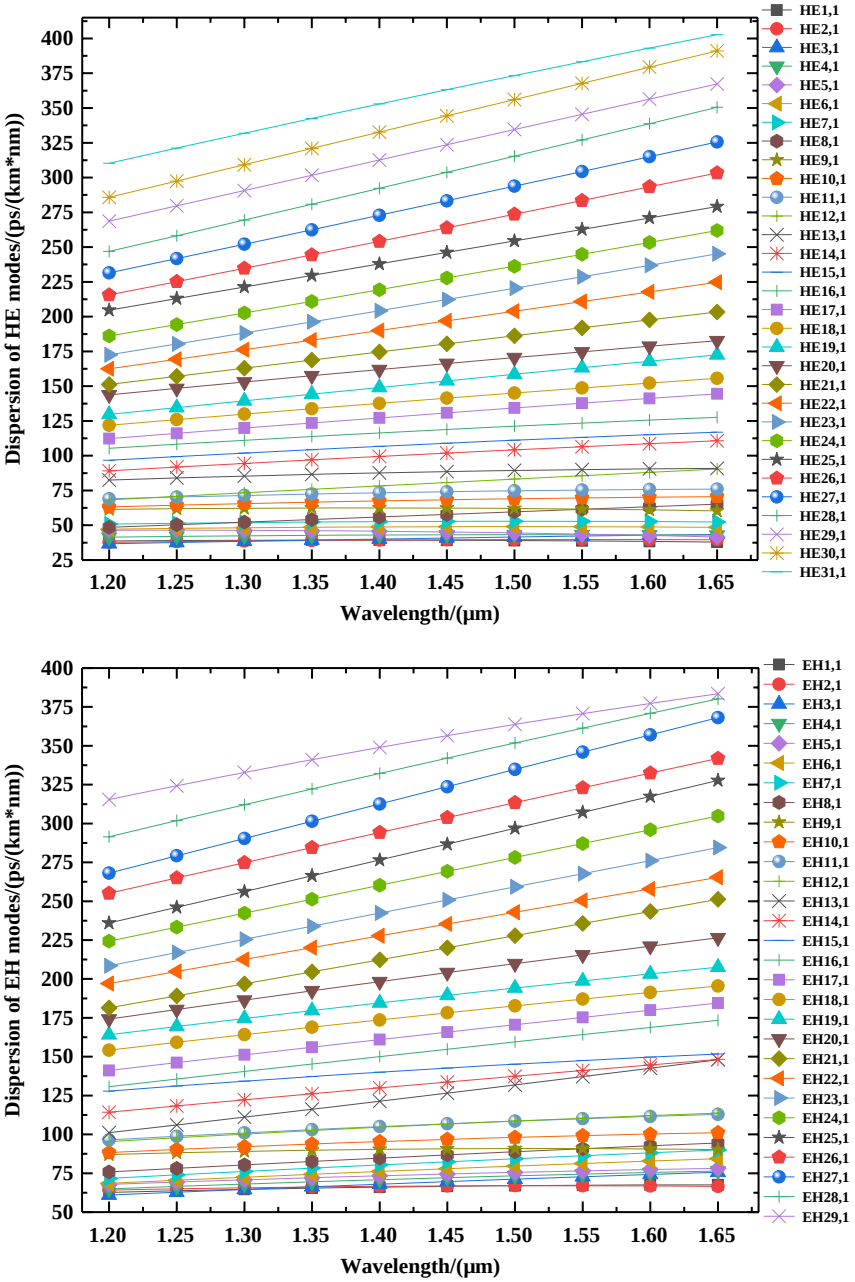

Fig. 5 Dispersion of the HE and EH modes.

$$\gamma = \frac{2\pi}{\lambda} \iint_S n_2(x,y) i^2(x,y) \mathrm{d}x\, \mathrm{d}y, \tag{6}$$

$$i(x,y) = \frac{\mathrm{Re}\left[\frac{\overline{E} \times \overline{H}^*}{2} \bullet \hat{z}\right]}{\iint_S \mathrm{Re}\left[\frac{E_x H_y^* - E_y^* H_x}{2}\right] \mathrm{d}x\, \mathrm{d}y}, \tag{7}$$

where $n_2\ (x,y) = 2.6 \times 10^{-20}\ \mathrm{m^2\,W^{-1}}$[12] and $n_2\ (x,y) = 2.3 \times 10^{-20}\ \mathrm{m^2\,W^{-1}}$[24] are used to calculate the nonlinear coefficients of the annular region and cladding, respectively. Figure 7 shows the nonlinear coefficients of the HE and EH modes. The longer the wavelength, the smaller is the nonlinear coefficient. The smallest nonlinear coefficient is 0.583 $\mathrm{W^{-1}\,km^{-1}}$ at 1.55 μm for $\mathrm{HE}_{31,1}$. It is 0.536 $\mathrm{W^{-1}\,km^{-1}}$ for $\mathrm{HE}_{31,1}$ in the whole band and lower than

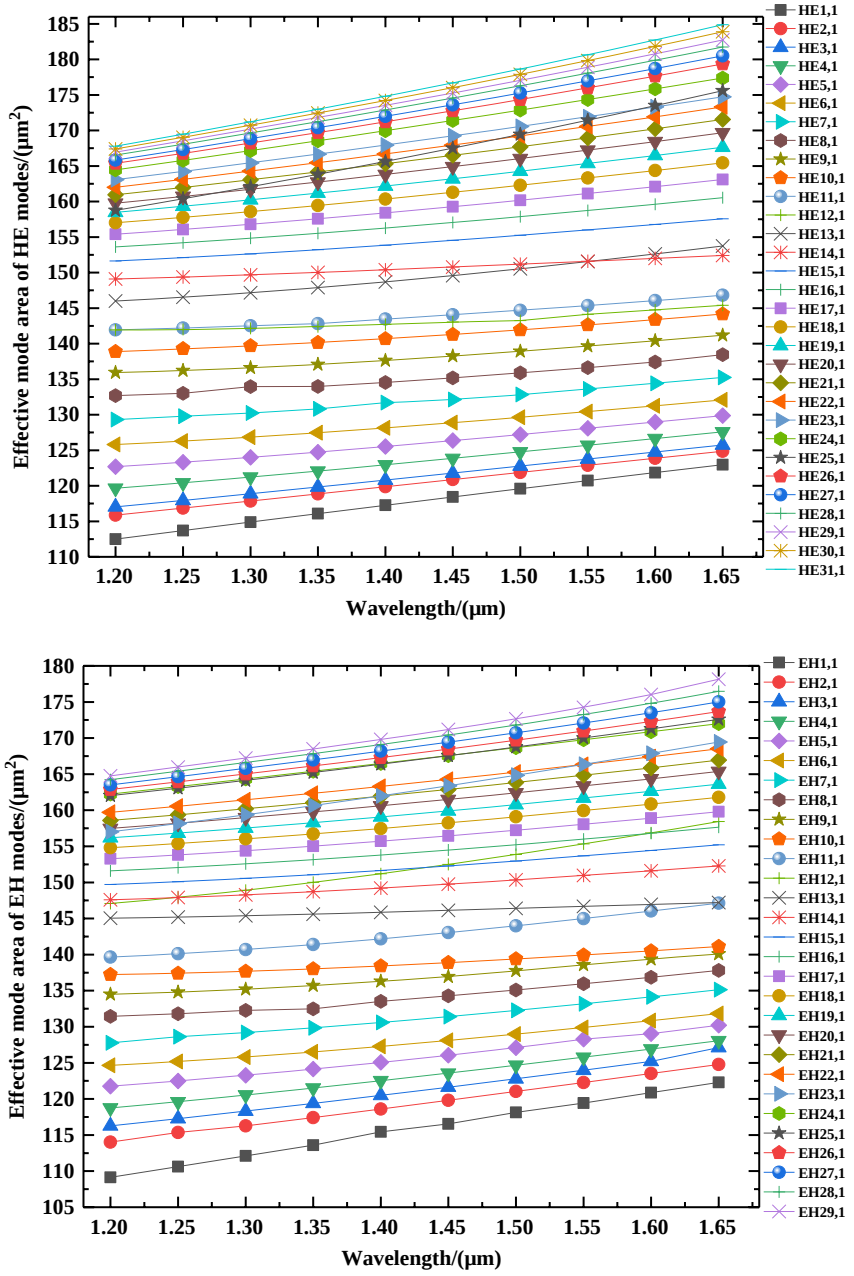

Fig. 6 Effective mode areas of the HE and EH modes.

1.032 $W^{-1} \cdot km^{-1}$ in Ref. 25 and 1.956 $W^{-1} \cdot km^{-1}$ in Ref. 26. In other words, in the 1.2 to 1.65 μm range, the nonlinear coefficient is very small (<1.25 $W^{-1}\,km^{-1}$) and very conducive to propagation of OAM modes in the fiber.

3.5 *Confinement Loss*

The confinement loss is an important issue and is described by Eq. (8):[27]

$$L = \frac{2\pi}{\lambda}\frac{20}{\ln(10)}10^6\,\mathrm{Im}(n_{\mathrm{eff}}), \tag{8}$$

where λ is the wavelength and $\mathrm{Im}(n_{\mathrm{eff}})$ is the imaginary part of the effective refractive index which can be calculated by COMSOL. The confinement loss can be adjusted by the air holes in

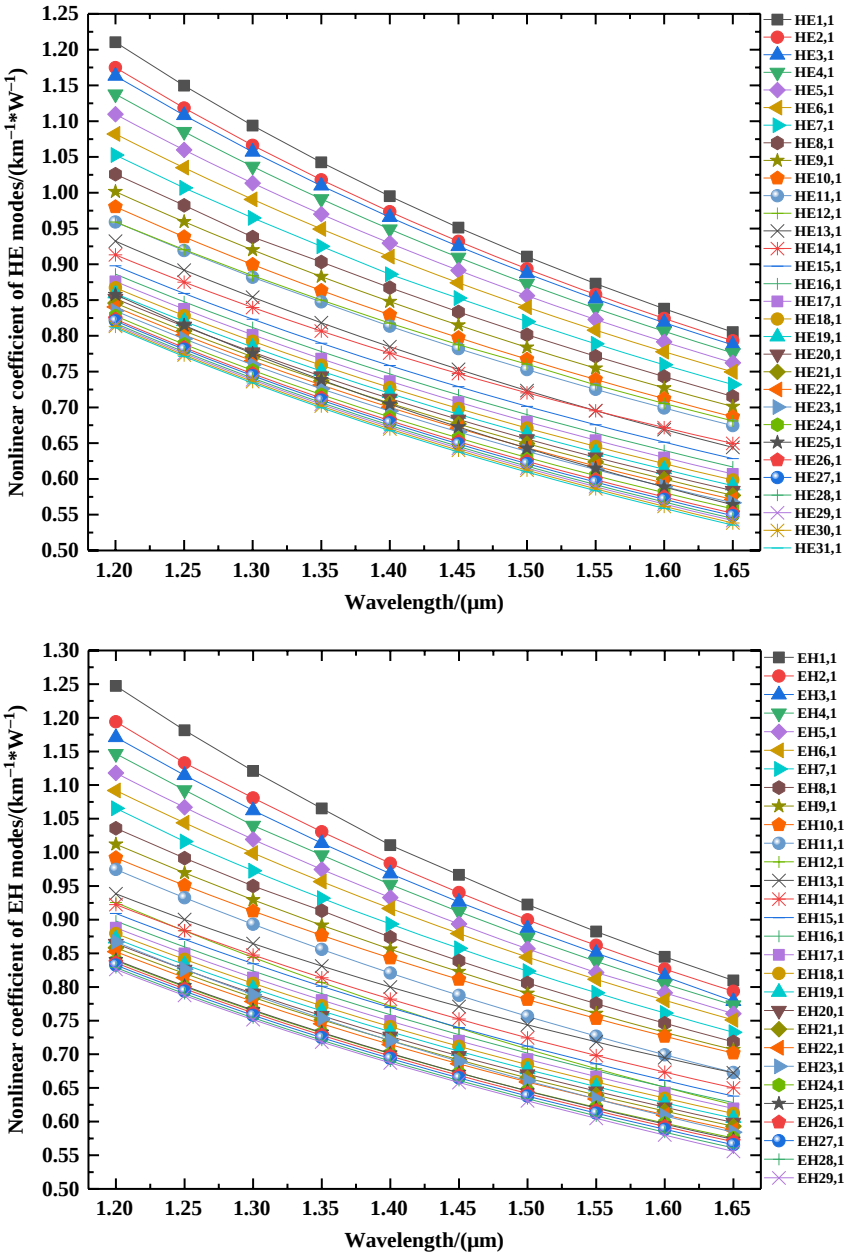

Fig. 7 Nonlinear coefficients of the HE and EH modes.

the cladding. Table 1 shows the confinement losses of all the eigenmodes at 1.55 μm and all the values of the OAM modes have the magnitude of 10^{-12} and 10^{-8} dB/m, which are lower than those in Ref. 28.

4 Conclusion

A new circular PCF is designed to support transmission of 118 OAM modes in the range of 1.2 to 1.65 μm. This number is the largest reported so far. Numerical simulation reveals that all the eigenmodes index differences are larger than 10^{-4} which can avoid the degeneracy between the patterns. Not only does this fiber has very large effective mode areas (180.65 μm^2 for the HE modes at 1.55 μm) and low nonlinear coefficient (0.583 $W^{-1}\,km^{-1}$ at 1.55 μm), but also dispersion is very flat [as low as 1.459 ps/(km · nm)]. Moreover, the loss of all the modes is very low and between 10^{-12} and 10^{-8}. This new PCF structure can improve the optical fiber

Table 1 The confinement losses of all the eigenmodes at 1.55 μm.

Modes	Confinement loss/(dB/m)	Modes	Confinement loss/(dB/m)	Modes	Confinement loss/(dB/m)	Modes	Confinement loss/(dB/m)
$HE_{1,1}$	6.99×10^{-10}	$HE_{17,1}$	3.29×10^{-12}	$EH_{1,1}$	4.70×10^{-09}	$EH_{17,1}$	3.97×10^{-09}
$HE_{2,1}$	4.42×10^{-09}	$HE_{18,1}$	1.30×10^{-09}	$EH_{2,1}$	2.57×10^{-09}	$EH_{18,1}$	3.35×10^{-10}
$HE_{3,1}$	8.35×10^{-09}	$HE_{19,1}$	4.24×10^{-09}	$EH_{3,1}$	3.28×10^{-09}	$EH_{19,1}$	2.36×10^{-09}
$HE_{4,1}$	7.69×10^{-10}	$HE_{20,1}$	9.59×10^{-09}	$EH_{4,1}$	1.51×10^{-09}	$EH_{20,1}$	5.06×10^{-09}
$HE_{5,1}$	1.11×10^{-08}	$HE_{21,1}$	7.18×10^{-09}	$EH_{5,1}$	7.69×10^{-09}	$EH_{21,1}$	1.24×10^{-08}
$HE_{6,1}$	4.91×10^{-09}	$HE_{22,1}$	1.57×10^{-08}	$EH_{6,1}$	8.43×10^{-10}	$EH_{22,1}$	5.60×10^{-09}
$HE_{7,1}$	4.09×10^{-09}	$HE_{23,1}$	8.63×10^{-09}	$EH_{7,1}$	1.26×10^{-08}	$EH_{23,1}$	9.91×10^{-09}
$HE_{8,1}$	2.86×10^{-09}	$HE_{24,1}$	1.78×10^{-08}	$EH_{8,1}$	2.20×10^{-09}	$EH_{24,1}$	1.09×10^{-08}
$HE_{9,1}$	1.94×10^{-09}	$HE_{25,1}$	9.99×10^{-09}	$EH_{9,1}$	6.87×10^{-10}	$EH_{25,1}$	2.58×10^{-08}
$HE_{10,1}$	5.36×10^{-09}	$HE_{26,1}$	4.09×10^{-08}	$EH_{10,1}$	1.18×10^{-08}	$EH_{26,1}$	2.33×10^{-09}
$HE_{11,1}$	9.10×10^{-09}	$HE_{27,1}$	1.05×10^{-08}	$EH_{11,1}$	5.05×10^{-09}	$EH_{27,1}$	1.75×10^{-08}
$HE_{12,1}$	4.29×10^{-09}	$HE_{28,1}$	2.31×10^{-08}	$EH_{12,1}$	4.59×10^{-09}	$EH_{28,1}$	7.96×10^{-09}
$HE_{13,1}$	1.06×10^{-08}	$HE_{29,1}$	1.57×10^{-09}	$EH_{13,1}$	3.74×10^{-11}	$EH_{29,1}$	2.69×10^{-08}
$HE_{14,1}$	6.66×10^{-09}	$HE_{30,1}$	1.41×10^{-08}	$EH_{14,1}$	7.25×10^{-11}	—	—
$HE_{15,1}$	5.86×10^{-09}	$HE_{31,1}$	8.50×10^{-09}	$EH_{15,1}$	4.72×10^{-11}	—	—
$HE_{16,1}$	3.92×10^{-09}	—	—	$EH_{16,1}$	2.66×10^{-10}	—	—

communication capacity and stability for multi-mode transmission and has large practical potential. In addition, we will continue to optimize the structure by focusing on the annular region and air holes in further research because the performance of proposed fiber is mainly depending on the thickness of the circular region and the shape, size, or location of the air holes in cladding.

Acknowledgments

This work was jointly supported by Local Universities Reformation and Development Personnel Training Supporting Project from Central Authorities (Grant No. 140119001), City University of Hong Kong Strategic Research Grant (SRG) (Grant Nos. 7005105 and 7005265), and Scientific Research Fund of Sichuan Province Science and Technology Department (Grant No. 2020YJ0137).

References

1. Y. Chen et al."Crosstalk-aware routing, spectrum, and core assignment in space-division multiplexing networks with bidirectional multicore fibers," *Opt. Eng.* **58**(11), 116110 (2019).
2. J. Wang et al., "Multiple orbital angular momentum (OAM) modes (De) multiplexer based on single complex phase mask," in *Eur. Conf. Opt. Commun.* (2014).
3. E. Liu et al., "Robust transmission of orbital angular momentum mode based on a dual-cladding photonic quasi-crystal fiber," *J. Phys. D: Appl. Phys.* **52**(32), 325110 (2019).
4. W. Huang et al., "A photonic crystal fiber for supporting 30 orbital angular momentum modes with low dispersion," *Optoelectron. Lett.* **16**(1), 34–39 (2020).
5. L. X. Wang et al., "Orbital-angular-momentum polarization mode dispersion in optical fibers," *J. Lightwave Technol.* **34**, 1661–1671 (2016).

6. Y. Yue, et al., "Octave-spanning super continuum generation of vortices in a As_2S_3 ring photonic crystal fiber," *Opt. Lett.* **37**(11), 1889–1891 (2012).
7. H. Li et al., "Guiding terahertz orbital angular momentum beams in multimode Kagome hollow-core fibers," *Opt. Lett.* **42**(2), 179–182 (2017).
8. A. Nandam and W. Shin, "Spiral photonic crystal fiber structure for supporting orbital angular momentum modes," *Optik* **169**, 361–367 (2018).
9. W. Tian et al., "A circular photonic crystal fiber supporting 26 OAM modes," *Opt. Fiber Technol.* **30**, 184–189 (2016).
10. M. Kim and S. Kim, "Epsilon-near-zero photonic crystal fibers for a large mode separation of orbital angular momentum modes," *Optik* **204**, 164209 (2020).
11. X. Bai et al., "Circular-lattice photonic crystal fiber with square air holes supporting 58 OAM modes," in *Prog. Electromagn. Res. Symp. – Spring*, pp. 3105–3108 (2017).
12. L. Zhang et al., "Circular photonic crystal fiber supporting 110 OAM modes," *Opt. Commun.* **429**, 189–193 (2018).
13. M. Ahabboud et al., "Effect of Cu doping on structural and dielectric properties of Pb1-xCux(Zr0.52Ti0.48)O3(PCxZT) ($0 \leq x \leq 0.2$) ceramics prepared by sol-gel method," *Asian J. Chem.* **33**(3), 665–670 (2021).
14. V. Matejec et al., "Performance of the sol-gel method for the preparation of optical fibers," *Rev. Roumaine Chim.* **52**(10), 991 (2007).
15. C. Liu et al., "Design and theoretical analysis of a photonic crystal fiber based on surface plasmon resonance sensing," *J. Nanophotonics* **9**(1), 093050 (2015).
16. H. Zhang et al., "A new type circular photonic crystal fiber for orbital angular momentum mode transmission," *IEEE Photonics Technol. Lett.* **28**(13), 1426–1429 (2016).
17. M. A. Kabir et al., "Novel spider web photonic crystal fiber for robust mode transmission applications with supporting orbital angular momentum transmission property," *Opt. Quantum Electron.* **52**(7), 331 (2020).
18. R. D. Shannon, "Refractive index and dispersion of fluorides and oxides," *J. Phys. Chem. Ref. Data* **31**(4), 931–970 (2002).
19. Y. Lei et al., "Numerical analysis of a photonic crystal fiber for supporting 76 orbital angular momentum modes," *J. Opt.* **20**, 105701 (2018).
20. B. Charles et al., "Design, fabrication and validation of an OAM fiber supporting 36 states," *Opt. Express* **22**(21), 26117–26127 (2014).
21. M. M. Hassan et al., "Numerical analysis of circular core shaped photonic crystal fiber for orbital angular momentum with efficient transmission," *Appl. Phys. B: Lasers Opt.* **126**(9), 145 (2020).
22. F. Poli et al., "Optical parametric amplification in all-silica triangular-core photonic crystal fibers," *Appl. Phys. B* **81**(2), 251–255 (2005).
23. M. Fuochi et al., "Study of Raman amplification properties in triangular photonic crystal fibers," *J. Lightwave Technol.* **21**, 2247–2254 (2003).
24. X. Wan et al., "Low dispersion and confinement loss photonic crystal fiber for orbital angular momentum mode transmission," *Opt. Quantum Electron.* **52**(6), 289 (2020).
25. X. Bai et al., "A new type Bragg fiber for supporting 50 orbital angular momentum modes," *Optik* **219**, 165153 (2020).
26. X. Bai et al., "Design of a circular photonic crystal fiber with square air-holes for orbital angular momentum modes transmission," *Opt. Zeitschr. Licht Elektronenoptik: = J. Light Electronoptic* **158**, 1266–1274 (2018).
27. Y. Qin et al., "Broadband and low confinement loss photonic crystal fibers supporting 48 orbital angular momentum modes," *Proc. SPIE* **11052**, 110520S (2019).
28. H. Zhang et al., "A design strategy of the circular photonic crystal fiber supporting good quality orbital angular momentum mode transmission," *Opt. Commun.* **397**, 59–66 (2017).

Haihao Fu is a graduate student of Northeast Petroleum University.

Chao Liu is a professor of Northeast Petroleum University.

Biographies of the other authors are not available.